ADVANCED MATERIALS INTERFACES
www.advmatinterfaces.de

In Situ (Operando) Electrochemical Dilatometry as a Method to Distinguish Charge Storage Mechanisms and Metal Plating Processes for Sodium and Lithium Ions in Hard Carbon Battery Electrodes

*Ines Escher, Guillermo A. Ferrero, Mustafa Goktas, and Philipp Adelhelm**

In situ (operando) electrochemical dilatometry (ECD) provides information on the expansion/shrinkage of an electrode during cell cycling. It is shown that the ECD signal can be used as descriptor to characterize the charge storage behavior of lithium and sodium ions in hard carbon electrodes. It is found that sodium storage in hard carbons occurs by a three-step mechanism, namely I) insertion, II) pore filling, and III) plating. Step III can be seen from a sudden increase in electrode thickness for potentials below around 36 mV versus Na^+/Na and is assigned to plating on the hard carbon surface. Interestingly, this last step is absent in the case of lithium which demonstrates that the storage behavior between both alkali metals is different. The plating mechanism is also supported by reference experiments in which bulk plating is enforced. Bulk plating on hard carbon electrodes can be detected more easily for sodium compared to lithium. It is also found that the type of binder strongly influences the dilatometry results. A comparison between the binders sodium salt of carboxymethyl cellulose and poly(vinylidene difluoride) shows that the use of the former leads to notably smaller first electrode expansion as well as a higher initial Coulomb efficiency.

1. Introduction

Sodium-ion batteries (SIBs) are among the most promising alternatives to lithium-ion batteries (LIBs).[1] The main driving force for developing SIBs is to develop energy stores based on more abundant elements with only little penalty in energy density compared to LIBs. While research on cathodes is focused on Mn- and/or Fe-rich compounds, a peculiarity for anodes is that graphite, the most common anode in LIBs, shows only a marginal capacity.[1a] This is because sodium-rich binary graphite intercalation compounds (Na_xC) are, in contrast to other alkali metals, thermodynamically instable.[2] A way around this problem is to co-intercalate solvent molecules along with sodium ions but the capacity for battery application still needs to be improved.[3] Because of this, much research is dedicated to the so-called hard carbons, which show a redox potential close to Na^+/Na and a storage capacity, depending on the exact type of hard carbon, typically between 150 and 350 mAh g^{-1}.[1d,g,4] Even higher values of 478 mAh g^{-1} are possible for tailor-made carbons as recently demonstrated by Kamiyama et al.[5]

Considering the charge storage of sodium ions in hard carbon, generally two regions in the voltage profile can be distinguished: I) a sloping region until around 0.1 V and II) a plateau region at lower voltage (<0.1 V). Despite numerous publications on sodium storage in hard carbon electrodes in recent years, the related storage mechanism is still a matter of debate. The most important reason for this is the structural complexity of hard carbons which aggravates their analysis and the comparison between different studies. While graphite is the thermodynamically stable and hence fully crystalline structure of carbon under ambient conditions (ideally only sp^2 hybridization), hard carbons show a lot of disorder (typically sp^2 and sp^3 hybridization in various ratios depending on the degree of disorder), they are porous (open and closed porosity) and contain other elements (mostly H, O, N, S) as impurities or, if intentionally added, as dopants. Structural models can be used to describe the carbon microstructure though it remains impossible to include all possible parameters.[6] Another aspect that complicates the discussion is that there is no consistent use of the relevant terminology. Generally, three different mechanisms are used to discuss the sodium storage in hard carbon: 1) insertion in graphitic domains,[7] which includes the intercalation between graphene sheets with a higher interlayer distance compared to graphite (0.335 nm);[1d,e,8] for interlayer distances

I. Escher, Dr. G. A. Ferrero, Dr. M. Goktas, Prof. P. Adelhelm
Institut für Chemie
Humboldt Universität zu Berlin
Brook-Taylor-Str. 2, 12489 Berlin, Germany
E-mail: philipp.adelhelm@hu-berlin.de
Prof. P. Adelhelm
Joint Research Group Operando Battery Analysis
Helmholtz-Zentrum Berlin
Hahn-Meitner-Platz 1, 14109 Berlin, Germany

The ORCID identification number(s) for the author(s) of this article can be found under https://doi.org/10.1002/admi.202100596.

DOI: 10.1002/admi.202100596

above 0.4 nm, the term adsorption rather than insertion is suggested;[9] 2) adsorption on defects[1d,e,8a,10], including the adsorption on heteroatoms;[1e,11] and 3) filling of pores[1d,e,12] in addition to the formation of quasi-metallic clusters.[13] The extent of the different sodium storage mechanisms depends on the exact properties of carbon material used. Once the electrode potential drops below 0 V versus Na^+/Na, plating of bulk sodium and dendrite growth takes place as fourth mechanism.[14]

One of the most accepted mechanism, first published by Stevens and Dahn, is that the sloping region in the voltage profile corresponds to sodium-ion insertion in the graphitic domains and the plateau region corresponds to pore filling.[15] This assumption was further proved and corroborated by using X-ray methods (small angle X-ray scattering, wide angle X-ray scattering) and Raman spectroscopy.[8b,12b,16] On the other hand, Zhang et al. did not observe an insertion mechanism based on X-ray diffraction measurements. They claimed that the sloping region can be correlated to an adsorption on heteroatoms (>1 V) and on the surface of the graphene sheets (1–0.1 V). According to them, a filling of mesopores is taking place in the plateau region.[17] Another mechanism was suggested by Cao et al. who ascribed the sloping region to the storage of sodium ions on the surface of small graphitic clusters (adsorption) and the plateau region to the insertion in the graphitic region by using theoretical calculations.[18] Different groups supported this mechanism by investigating the influence of synthesis parameters on the voltage profile[10a,19] and/or using different additional characterization techniques like X-ray diffraction (XRD),[19b] NMR spectroscopy,[19b] electron paramagnetic resonance spectroscopy,[19b] as well as theoretical calculations.[19] Overall, most of the studies distinguished the storage mechanism into two regions that are clearly visible in the voltage profile.[8b,15,17–19]

In addition, other studies subdivide the final plateau again into two regions: an upper voltage plateau that provides mostly the majority of the capacity and a lower voltage plateau that contributes to a minor fraction. The upper plateau is ascribed to insertion between the graphene layers[8a,20] whereas the lower plateau is correlated to pore filling[8a,20] with gradual change of the chemical state of adsorbed sodium to sodium metal.[8a]

In the case of lithium, the voltage profile of the ion intercalation into hard carbon can mostly be divided into two regions (sloping and plateau) as well. Herein, the storage mechanism is also still under debate and different mechanisms for the sloping region like insertion between graphene layers[16] or adsorption[11,21] are proposed. For the plateau region, insertion between the layers,[11,21] adsorption on single layer graphene sheets,[22] as well as lithium-ion storage via pore filling,[16] especially the formation of quasi-metallic clusters[23] or lithium metal[24] within those pores are proposed. A major difference between the use of hard carbons in LIBs and SIBs is the correlation between the plateau capacity and the carbonization temperature. While for SIBs the plateau capacity increases with increasing carbonization temperature, for LIBs the plateau capacity goes through a maximum at 1300 °C.[25]

From the above paragraphs, it is clear that the storage behavior of hard carbons is intrinsically complex and understanding of the underlying processes requires insight from several analytical tools. In situ or operando XRD would be the natural choice but the large disorder of hard carbons aggravates the analysis. Here, we apply in situ electrochemical dilatometry (ECD) as a method to follow the sodiation/desodiation of hard carbon electrodes and compare the results to the analog reaction with lithium. The method probes the change in electrode thickness during cycling ("breathing") which can be linked to different storage mechanisms and phase transitions.[26] The method is often referred as in situ method but it is important to realize that the actual mode of operation is operando, i.e., the electrode thickness is continuously measured (typically during a constant current experiment). The device operates with a three-electrode geometry which mitigates potential issues due to the metal counter electrode.[27] In addition, diglyme was used as electrolyte solvent in this study as it shows a favorable solid electrolyte interphase (SEI) formation as well as better charge delivery in hard carbon electrodes.[13b] Recently, we demonstrated that ECD can be used for studying sodium storage in a specialized hard carbon structure.[28] However, we were not able to fully interpret the data due to the lack of more systematic data and the missing comparison to the analog experiment with lithium. In addition, the type of binder also influences the ECD signal, as recently shown for graphite electrodes by our group[26c] as well as having an effect on the cycling behavior of hard carbon electrodes as proven by Dahbi et al.[29] This study therefore also includes a comparison for the two common binders, sodium salt of carboxymethyl cellulose (CMC) and poly(vinylidene difluoride) (PVDF). An overview of our major findings regarding the storage mechanisms is shown in **Scheme 1**.

2. Results and Discussion

The hard carbon used in this study was provided by Kureha Corporation and has been developed for battery applications. Information on the specific carbon (Carbotron P(J)) can be found in Figure S1 (Supporting Information). The ECD experiments were conducted using an ECD-3-nano device from El-Cell. The cells were galvanostatically cycled at a current density of 10 mA g^{-1} in a climate chamber at 25 °C. The variation in electrode thickness was recorded using a capacitive sensor, the detection limit is ≤5 nm. A solution of 1 M $NaPF_6$ or 1 M LiOTf in 2G was used as electrolyte. The electrodes contained 85 w/w active material, 10 w/w binder, and 5 w/w conductive carbon black (see the Experimental Section for more details).

2.1. Initial Cycle and Influence of Binder

The initial charge/discharge cycle as well as the dilatometry experiments strongly depend on the type of binder, as shown in **Figure 1** for PVDF and CMC. As can be observed in Figure 1a,b, the potential profiles showed a sloping region until 0.1 V followed by a plateau region when the potential is below 0.1 V. Differences on the thickness and potential profiles can be clearly observed between hard carbon and graphite, as can be compared with the previous studies published by our group.[26a,c,30] A periodically increase and decrease of up to 100% during cycling was measured for the graphite electrode due to the well-known co-intercalation reaction of sodium ions with ether-based electrolytes.[26a,c,30,31] Since the hard carbon electrodes consist of locally ordered regions, one

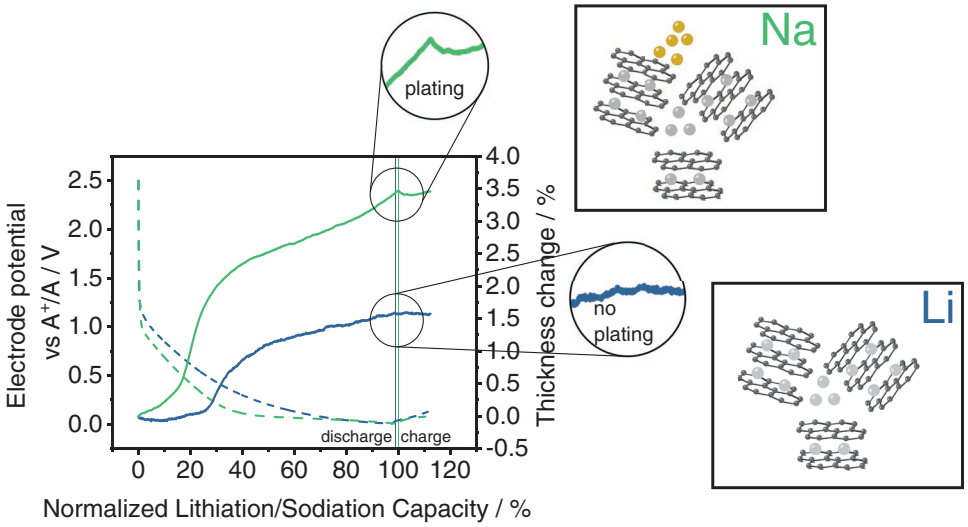

Scheme 1. Schematic illustration of the main results regarding the different storage mechanisms of sodium and lithium ions in hard carbon.

could imagine that a certain co-intercalation reaction also takes place here. However, as can be shown in Figure 1, this is not the case and a maximal electrode expansion of 6.1% in the first cycle is detected here, i.e., solvent co-intercalation is unlikely. Compared to the increase observed for the graphite electrodes, it can be inferred that sodium ions can be introduced into this expanded graphite lattice without the need of a co-intercalation reaction. This phenomena will occur when the interlayer distance is higher than 0.36 nm,[9] and therefore it will allow the use of hard carbon electrodes with carbonate-based electrolytes as well.[8b,12a,32]

More importantly, the data clearly show the dramatic influence of the type of binder. While the initial thickness increment for the PVDF-based electrode is 6.1%, only 0.8% is recorded in case of CMC. A similar behavior is observed for lithium cells (4.5% versus 1.9%) likewise the results obtained for graphite electrodes.[26c] These results can be ascribed to the higher tolerance against internal mechanical stress by the nonfluorinated binders compared to fluorinated ones (e.g., PVDF).[33]

In addition, the initial Coulomb efficiency (ICE) in the first cycle for the electrodes made with PVDF is lower compared

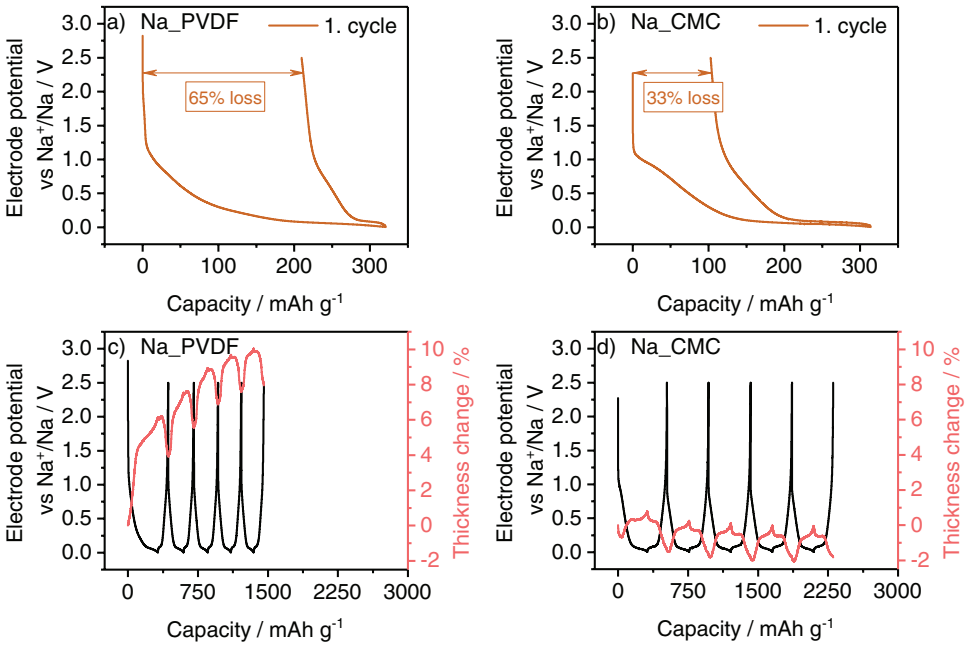

Figure 1. In situ electrochemical dilatometry experiments of hard carbon with two different binders (a,c) PVDF, b,d) CMC) in sodium-ion batteries (10 mA g^{-1}). Loading and initial thickness without current collector of Na_PVDF 2.2 mg cm^{-2}, 33.3 µm, Na_CMC 2.6 mg cm^{-2}, 46.3 µm. Three-electrode set-up with sodium as counter and reference electrode. 1 M $NaPF_6$ in diglyme as electrolyte. a) and b) Hysteresis plot of the 1st cycle and capacity loss, c) and d) electrode potential and thickness change of five cycles.

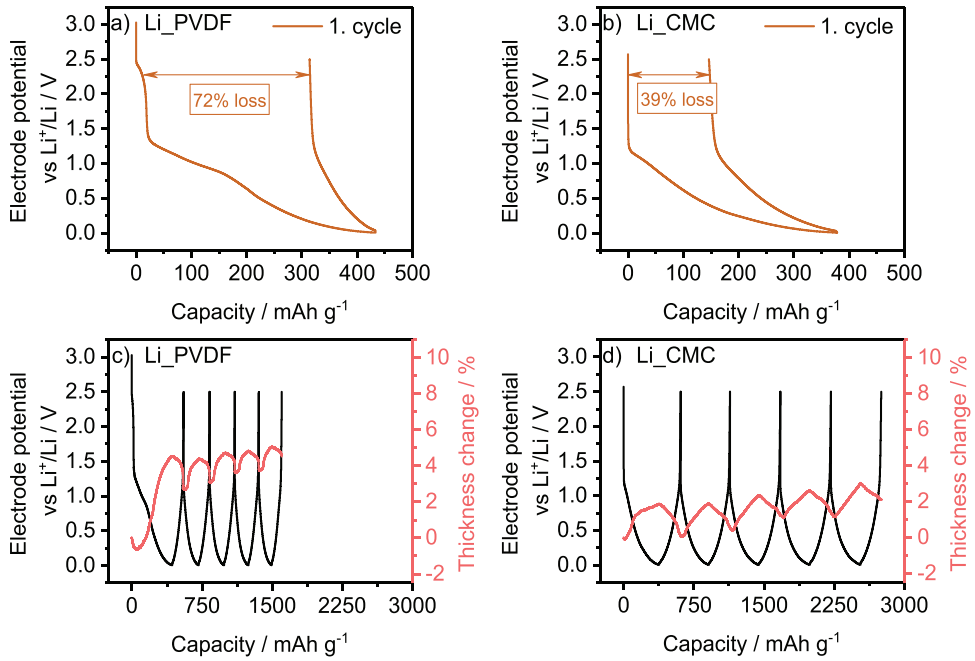

Figure 2. In situ electrochemical dilatometry experiments of hard carbon with two different binders (a,c) PVDF, b,d) CMC) in lithium-ion batteries (10 mA g^{-1}). Loading and initial thickness without current collector of Li_PVDF 1.9 mg cm^{-2}, 30.3 µm, Li_CMC 1.6 mg cm^{-2}, 34.3 µm. Three-electrode set-up with lithium as counter and reference electrode. 1 M LiOTf in diglyme as electrolyte. a) and b) Hysteresis plot of the 1st cycle and capacity loss, c) and d) electrode potential and thickness change of five cycles.

to the ones made with CMC (Na_PVDF: 35% and Li_PVDF: 28% versus Na_CMC: 67% and Li_CMC: 61%, see **Figures 1** and **2**). The high initial thickness increase and the low ICE are the result of side reactions that appear stronger in case of PVDF electrodes. The lower ICE of PVDF-based electrodes can be also corroborated in rate capability tests performed in a two-electrode set-up shown in Figures S2 and S3 (Supporting Information). As previously observed by Dahbi et al., the electrolyte decomposition is suppressed in the case of CMC, while a loosening of the hard carbon particles occurred when fluorinated binders are used due to defluorination of the binder material. Unlike their work, an improvement effect was here found for both SIBs and LIBs.[29] The difference is likely due to the different types of solvents used in both studies (propylene carbonate versus diglyme) which lead to a different SEI formation.[34]

2.2. Differences between Lithium and Sodium Storage

The storage mechanism was further elucidated from the second cycle of the in situ ECD experiments using PVDF as binder material as the data were more reproducible over multiple cycles. **Figures 3** and **4** display the potential profiles and the change in electrode thickness for the sodium and lithium cells. The figures also show derivative plots of the thickness change (dl/dQ versus Q), which show more clearly differences during the measurement. In this manner, it is possible to distinguish between different regions.

The potential profile of the sodium cell consists of a sloping region above 0.1 V and a plateau region below 0.1 V, as commonly known from literature.[1d,4c] The thickness variation profile can be divided into three regions: I) a very rapid and dynamic thickness increase (varying values for dl/dQ but all >0), that correlates with the sloping region in the potential profile (green region); II) a region with constant and more intermediate increase (dl/dQ very small) that corresponds to the plateau region in the potential profile (blue region); and III) again a more rapid increase near the cut-off potential ($dl/dQ > 0$) (purple region). This three-step mechanism was also found by Alptekin et al.[28] for carbons carbonized up to 1500 °C. While this indicated that the behavior is general, we also note that we did not observe the third step starting from 1700 °C.[28]

The interesting point now is that, in contrast to literature that reports similar mechanisms for lithium and sodium,[16,35] our data show clear differences between both alkali metals. In the voltage profile, no plateau region is visible for lithium cells and the sloping region is prolongated (see Figure 4), whereas a clear division between two regions is visible for sodium cells in the original graphs (see Figure 3) as well as the derivative curve (Figure S4, Supporting Information). Although the derivative plots show the changes of the slope in a clearer way, almost no difference can be seen for lithium (Figure S5, Supporting Information). Even though the absence of the plateau region was already described in literature,[8b,11,36] it might appear when lower current densities are used or/and an additional constant voltage step is applied at the end.[11]

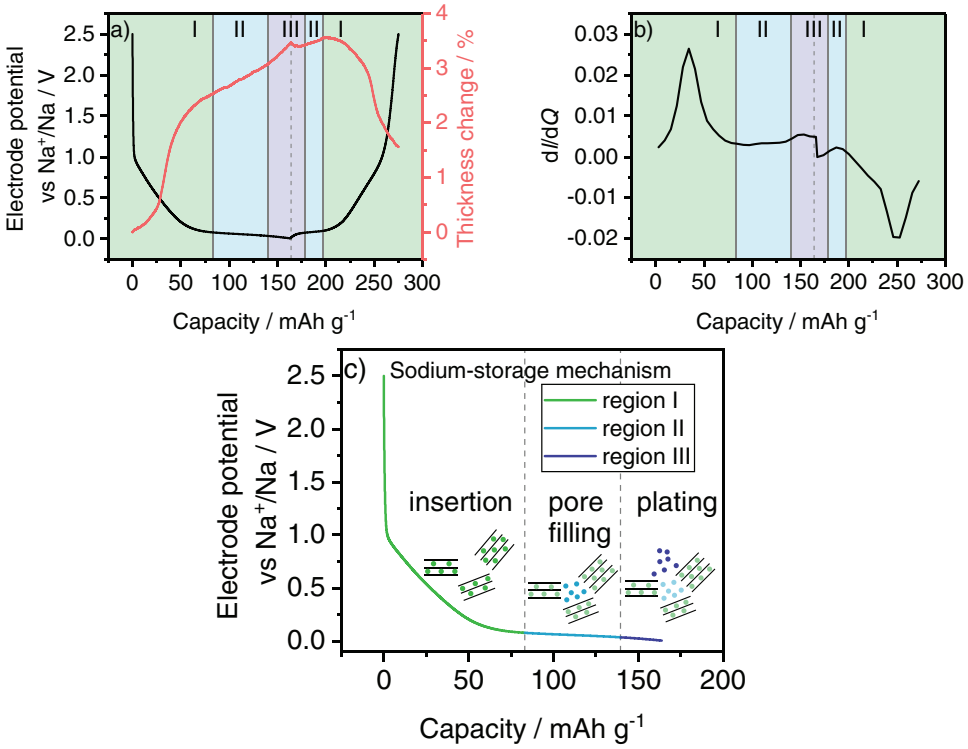

Figure 3. In situ electrochemical dilatometry experiments of hard carbon with PVDF as binder in sodium-ion batteries (second cycle, 10 mA g^{-1}). Three-electrode set-up with sodium as counter and reference electrode. 1 M $NaPF_6$ in diglyme as electrolyte. a) Electrode potential and thickness change, b) derivative of the thickness change, and c) proposed sodium-ion storage mechanism.

With regards to the thickness change, the results for sodium and lithium are very comparable despite their different ion sizes.[37] The main difference is the absence of thickness increase near the cut-off potential for the LIBs.

2.3. Linking Dilatometry Data to Storage Mechanisms and Metal Plating

Figures 3 and 4 clearly show that the different storage mechanisms in hard carbons can be followed by ECD measurements and that there are clear differences between lithium and sodium in the low voltage region close to 0 V versus A^+/A. While ECD does not provide direct evidence for the chemical state of lithium or sodium in the electrode, the method operates in operando mode and results may be linked to existing storage mechanisms proposed in literature. This means that in the case of sodium (Figure 3), the rapid thickness increase within the sloping potential region (green region, region I) can be linked to the insertion of sodium ions into graphitic domains (except the very first part of region I which might be due to strong interaction of sodium ions with heteroatoms rather than insertion). The rather small thickness increase within the plateau region at around 0.1 V (blue region, region II) could be then well explained with a pore filling mechanism. This is very reasonable because filling void space likely leads to less expansion compared to insertion between the graphene sheets in the graphitic domains. These two regions can be also distinguished in the case of lithium. Although no clear potential plateau is visible in this case, the ECD data suggest an overall comparable storage mechanism for lithium and sodium within regions I and II.

Region III (purple region) only appears in case of sodium which means the ECD data suggest an additional storage mechanism. Compared to region II, this region is characterized by a faster electrode expansion (shrinkage) during discharging (charging). We therefore link this region to plating (stripping) of sodium on the surface of the hard carbon. A similar behavior has been observed when CMC is used as binder (see Figures S6 and S7 in the Supporting Information). The fact that the plating takes place slightly above 0 V versus Na^+/Na (underpotential deposition) could be due to two reasons: first, the plated sodium is unstable compared to bulk sodium which could be the case for confined or nanoscopic structures; second, the electrode potential is locally already below 0 V, i.e., the conditions for bulk plating are reached.

Alvin et al.[8a] and Bommier et al.[20a] have already proposed an adsorption in pores mechanism on this last region. Both suggested a conversion from sodium ions to sodium metal at lower voltage values and therefore correlated the last region to a sodium-atom deposition on the surface of pores[20a] or the change of the adsorbed sodium ions in micropores to sodium metal below 0.1 V.[8a] Jin et al. also divided the voltage profile in three separate parts using galvanostatic intermittent titration technique experiments and correlated the last step between 0.03 and 0.01 V to the formation of sodium clusters in

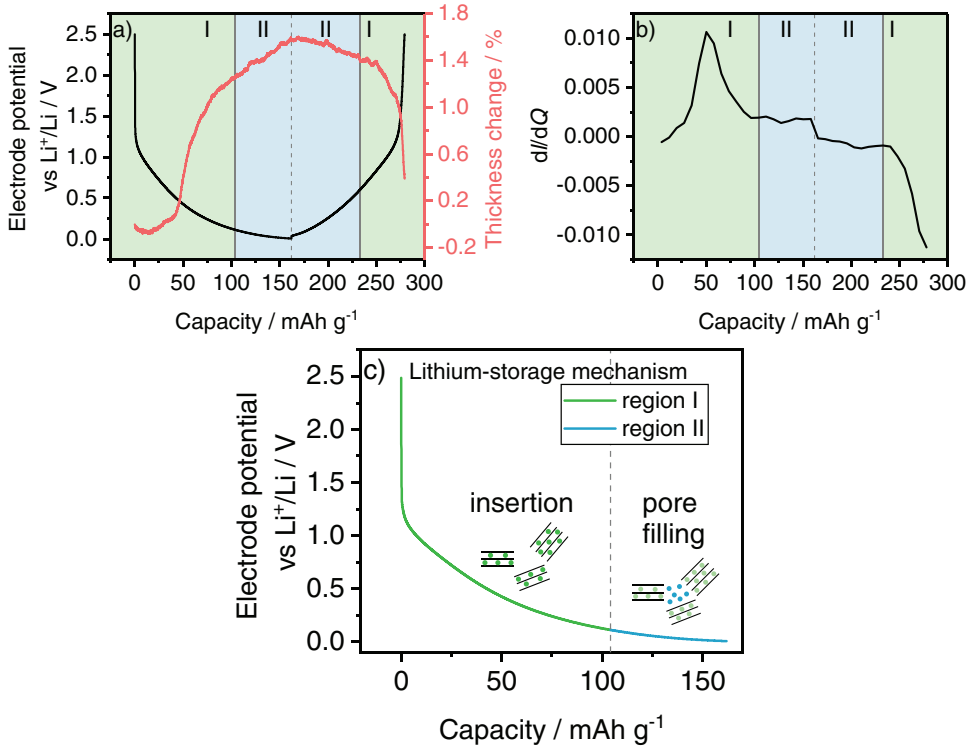

Figure 4. In situ electrochemical dilatometry experiments of hard carbon with PVDF as binder in lithium-ion batteries (second cycle, 10 mA g^{-1}). Three-electrode set-up with lithium as counter and reference electrode. 1 M LiOTf in diglyme as electrolyte. a) Electrode potential and thickness change, b) derivative of the thickness change, and c) proposed lithium-ion storage mechanism.

pores.[20b] This is in line with Lee et al. who proposed the formation of quasi-metallic nanoclusters at the end of discharge by using in situ XRD, ex situ field-emission transmission electron microscope, and ex situ X-ray photoelectron spectroscopy depth profiles.[13b]

A straightforward question is, how the increase in electrode thickness in region III compares to the situation of an ideal plating (= planar plating of sodium). The absolute expansion of the electrode in region III (sodiation) amounts to 0.14 µm with 0.0412 mAh of charge being stored. A charge of 0.0142 mAh corresponds to a sodium volume of 3.66×10^{-11} mm^3, i.e., planar plating of sodium would ideally increase the electrode thickness by 0.47 µm (see the Supporting Information for details). As the experimental value is lower, we assume that most plating takes place within the porous electrode structure. Note that several types of porosity (open, closed, or interparticular porosity) may account for this. Battery electrodes show a porosity of around 20–60%, depending on how they are processed which mitigates the expansion/shrinkage due to electrode reactions. A similar behavior has been observed for the expansion of Sn particles within a porous graphite electrode. In this case, the electrode expansion is also significantly smaller compared to what would be expected from the alloy formation.[38]

To further support the hypothesis that sodium plating takes place in region III, reference measurements with ECD were made for lithium and sodium cells for which bulk plating was forced by taking the electrode potential below 0 V. Results can be seen in **Figure 5**. In line with the results discussed in the previous section, the sodium cells show a sudden thickness increase starting at around 0.03 V, the beginning of region III. This thickness increase continues further with the same speed until the nucleation barrier for bulk plating is reached. From then on, the electrode expands further but the behavior is notably different to region III. This behavior is not observed in case of lithium, indicating that the underpotential metal plating in region III is specific to sodium. Moreover, the results show that bulk plating is more easily detectable in case of sodium compared to lithium.

The amount of charge that is stored in the lower plateau region counts to 30% of the whole plateau capacity, mostly values from 4% to 23% were shown in other publications using different characterization techniques.[8a,20a]

It has to be mentioned that this third region is neither visible in the normal potential profile nor in the derivative curve of the potential which means that there is barely an energetic difference between both mechanisms.

3. Conclusion

This study shows that different charge storage mechanisms in hard carbon for lithium and sodium can be followed by in situ ECD. For sodium, a three-step mechanism is confirmed. In the sloping region (region I, insertion), the electrode expansion is dynamic and fast. In the plateau region (region II, pore filling), the expansion is slower and relatively constant. Close

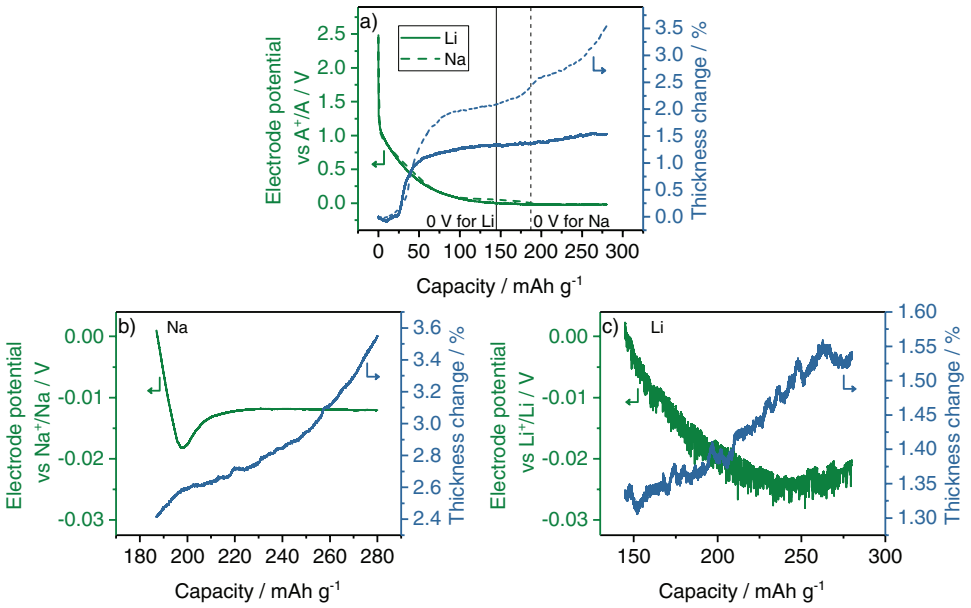

Figure 5. Plating experiment followed by in situ electrochemical dilatometry of hard carbon with PVDF as binder in sodium-ion batteries as well as lithium-ion batteries. Three-electrode set-up with sodium or lithium as counter and reference electrode, both cells precycled. 1 M $NaPF_6$ or 1 M LiOTf in diglyme as electrolyte. a) Electrode potential and thickness change, b) enlargement of the curve for the sodium-ion battery, and c) enlargement of the curve for the lithium-ion battery.

to the cut-off potential, however, the electrode expansion increases again, while no apparent differences in the potential profile are observed. This indicates a change in mechanism albeit with very similar thermodynamic driving force (pore filling followed by metal plating on the hard carbon surface). Most importantly, this additional process is only visible in case of sodium. Analog experiments with lithium did not show such a third region, indicating that the reaction mechanism for both alkali metals is different in this region, but similar in regions I and II.

Using CMC in comparison to PVDF as binder material shows a reduced electrode expansion in the first cycle as well as a higher ICE value, indicating more side reactions in the case of PVDF.

4. Experimental Section

Electrode Preparation: The electrodes were made from 85 w/w hard carbon Carbotron P(J) from Kureha Corporation, 5 w/w carbon black (IMERYS) as conductive additive, and 10 w/w binder. If PVDF (PI-KEM Ltd.) was used as binder, N-methylpyrrolidone (Sigma-Aldrich) was used as solvent, in the case of CMC (PI-KEM Ltd.), an aqueous solution was used. Electrodes were casted with an initial thickness of 300 µm, dried overnight on air, punched to the appropriate size (10 and 12 mm), and dried again at 110 °C under vacuum overnight. Electrode thicknesses were measured with a digital thickness dial gauge from Käfer Messuhrenfabrik GmbH.

Electrochemical Measurements: In situ ECD experiments were conducted with an ECD-3-nano cell from EL-CELL GmbH. This three-electrode set-up contained the alkali metal (sodium from BASF and lithium from Rockwood Lithium) as counter (12 mm diameter) and reference electrodes and the hard carbon electrode as working electrode (10 mm diameter). 1 M LiOTf (99.995% trace metal basis, Sigma-Aldrich) in diglyme (Sigma-Aldrich, predried with 4 Å molecular sieve) and 1 M $NaPF_6$ (>99%, Sigma-Aldrich) in diglyme were used as electrolyte, around 250 µL was used for each cell. Galvanostatic charge and discharge experiments with potential limitation (GCPL experiments) were conducted at a Biologic SP-50 battery cycler at 25 °C. The potential limit was set to 0.005–2.5 V versus Na^+/Na or Li^+/Li and a current of 10 mA g^{-1} was applied. For the plating experiments, the cut-off voltage was set to −0.1 V and the experiments were stopped when continuous plating was observed. Abbreviations used in the discussion related to the used alkali metal and binder (e.g., Na_PVDF).

The rate capability tests were conducted as two-electrode experiments in coin cells with the hard carbon electrode as working electrode and the particular alkali metal as counter electrode. Two glass microfiber filters (GF/A) from Whatman (diameter of 16 mm) were used as separator and were soaked with 100 µL of the electrolyte. GCPL experiments were carried out at a Biologic BCS 805 with a voltage window of 0.005–2.5 V versus Na^+/Na or Li^+/Li. Current rates of 10, 30, 50, 100, 200, 500, 1000, 2000, and again 10 mA g^{-1} were used and five full cycles were conducted for each current rate.

Physical and Chemical Characterization: Scanning electron microscope (SEM) images were taken with a scanning electron microscope (Phenom Pharos Desktop SEM, Phenom World) using an accelerating voltage of 15 kV and a secondary electron detector. XRD measurements were performed with a D2 Phaser instrument from Bruker. A Cu X-ray tube (30 kV, 10 mA) was used to conduct the experiments between 15° and 35°, using a step width of 0.05°. The nitrogen sorption isotherm was measured at −196 °C using a Quantachrome AUTOSORB-1. The pore volume as well as the pore size distribution was calculated applying the quenched-solid density functional theory method to the adsorption data, assuming a slit pore model. The Brunauer-Emmett-Teller (BET) surface area was calculated from a multipoint BET measurement in the relative pressure

range of 0.06–0.3. Elemental analysis was measured using a Euro EA 3000 from EuroVector S.P.A., values shown were the mean values of two measurements.

Supporting Information

Supporting Information is available from the Wiley Online Library or from the author.

Acknowledgements

This project has received funding from the Deutsche Forschungsgemeinschaft (DFG, German Research Foundation, Grant Nos. 298787956 and 325774457) and from the European Research Council (ERC) under the European Union's Horizon 2020 research and innovation programme (Grant Agreement No. 864698, SEED). The authors thank BASF for providing high purity sodium and Kureha Corp. for providing the hard carbon. The authors thank Dongjiu Xie (Group of Prof. Yan Lu) from the Helmholtz-Zentrum Berlin for the BET measurements. The authors thank Stefanie Markstein from the Humboldt Universität zu Berlin for the elemental analysis.

Open access funding enabled and organized by Projekt DEAL.

Conflict of Interest

The authors declare no conflict of interest.

Data Availability Statement

Research data are not shared.

Keywords

electrochemical dilatometry, hard carbon, lithium-ion batteries, sodium-ion batteries, storage mechanism

Received: April 12, 2021
Revised: June 3, 2021
Published online: July 20, 2021

[1] a) P. K. Nayak, L. Yang, W. Brehm, P. Adelhelm, *Angew. Chem., Int. Ed.* **2018**, *57*, 102; b) J.-Y. Hwang, S.-T. Myung, Y.-K. Sun, *Chem. Soc. Rev.* **2017**, *46*, 3529; c) G.-L. Xu, R. Amine, A. Abouimrane, H. Che, M. Dahbi, Z.-F. Ma, I. Saadoune, J. Alami, W. L. Mattis, F. Pan, Z. Chen, K. Amine, *Adv. Energy Mater.* **2018**, *8*, 1702403; d) X. Dou, I. Hasa, D. Saurel, C. Vaalma, L. Wu, D. Buchholz, D. Bresser, S. Komaba, S. Passerini, *Mater. Today* **2019**, *23*, 87; e) B. Xiao, T. Rojo, X. Li, *ChemSusChem* **2019**, *12*, 133; f) I. Hasa, S. Mariyappan, D. Saurel, P. Adelhelm, A. Y. Koposov, C. Masquelier, L. Croguennec, M. Casas-Cabanas, *J. Power Sources* **2021**, *482*, 228872; g) D. Saurel, B. Orayech, B. Xiao, D. Carriazo, X. Li, T. Rojo, *Adv. Energy Mater.* **2018**, *8*, 1703268; h) E. Goikolea, V. Palomares, S. Wang, I. R. de Larramendi, X. Guo, G. Wang, T. Rojo, *Adv. Energy Mater.* **2020**, *10*, 2002055.

[2] a) O. Lenchuk, P. Adelhelm, D. Mollenhauer, *Phys. Chem. Chem. Phys.* **2019**, *21*, 19378; b) H. Moriwake, A. Kuwabara, C. A. J. Fisher, Y. Ikuhara, *RSC Adv.* **2017**, *7*, 36550.

[3] B. Jache, P. Adelhelm, *Angew. Chem., Int. Ed.* **2014**, *53*, 10169.

[4] a) B. Yang, J. Wang, Y. Zhu, K. Ji, C. Wang, D. Ruan, Y. Xia, *J. Power Sources* **2021**, *492*, 229656; b) E. Irisarri, A. Ponrouch, M. R. Palacin, *J. Electrochem. Soc.* **2015**, *162*, A2476; c) L.-F. Zhao, Z. Hu, W.-H. Lai, Y. Tao, J. Peng, Z.-C. Miao, Y.-X. Wang, S.-L. Chou, H.-K. Liu, S.-X. Dou, *Adv. Energy Mater.* **2021**, *11*, 2002704.

[5] A. Kamiyama, K. Kubota, D. Igarashi, Y. Youn, Y. Tateyama, H. Ando, K. Gotoh, S. Komaba, *Angew. Chem., Int. Ed.* **2021**, *60*, 5114.

[6] a) P. Adelhelm, K. Cabrera, B. M. Smarsly, *Sci. Technol. Adv. Mater.* **2012**, *13*, 015010; b) K. Faber, F. Badaczewski, W. Ruland, B. M. Smarsly, *Z. Anorg. Allg. Chem.* **2014**, *640*, 3107; c) C. J. Jafta, A. Petzold, S. Risse, D. Clemens, D. Wallacher, G. Goerigk, M. Ballauff, *Carbon* **2017**, *123*, 440; d) K. Wang, Y. Jin, S. X. Sun, Y. Huang, J. Peng, J. Luo, Q. Zhang, Y. Qiu, C. Fang, J. Han, *ACS Omega* **2017**, *2*, 1687.

[7] IUPAC provides definitions for terms such as "graphitic", see, e.g., doi: https://doi.org/10.1351/goldbook.G02689 but the use in literature is not consistent. Nongraphitic carbons can be subdivided in hard carbons and soft carbons of which only the latter can be practically transformed to graphite by heat treatment. In this study, we report on a hard carbon but use the term "graphitic domains" to describe a local, more or less parallel stacking of a few graphene sheets in this otherwise nongraphitic material, https://doi.org/10.1351/goldbook.G02689 (accessed: June 2021).

[8] a) S. Alvin, D. Yoon, C. Chandra, H. S. Cahyadi, J.-H. Park, W. Chang, K. Y. Chung, J. Kim, *Carbon* **2019**, *145*, 67; b) S. Komaba, W. Murata, T. Ishikawa, N. Yabuuchi, T. Ozeki, T. Nakayama, A. Ogata, K. Gotoh, K. Fujiwara, *Adv. Funct. Mater.* **2011**, *21*, 3859.

[9] N. Sun, Z. Guan, Y. Liu, Y. Cao, Q. Zhu, H. Liu, Z. Wang, P. Zhang, B. Xu, *Adv. Energy Mater.* **2019**, *9*, 1901351.

[10] a) A. Gomez-Martin, J. Martinez-Fernandez, M. Ruttert, M. Winter, T. Placke, J. Ramirez-Rico, *Chem. Mater.* **2019**, *31*, 7288; b) Y. Li, Y.-S. Hu, M.-M. Titirici, L. Chen, X. Huang, *Adv. Energy Mater.* **2016**, *6*, 1600659.

[11] S. Alvin, H. S. Cahyadi, J. Hwang, W. Chang, S. K. Kwak, J. Kim, *Adv. Energy Mater.* **2020**, *10*, 2000283.

[12] a) P. Bai, Y. He, X. Zou, X. Zhao, P. Xiong, Y. Xu, *Adv. Energy Mater.* **2018**, *8*, 1703217; b) D. A. Stevens, J. R. Dahn, *J. Electrochem. Soc.* **2000**, *147*, 4428.

[13] a) J. M. Stratford, P. K. Allan, O. Pecher, P. A. Chater, C. P. Grey, *Chem. Commun.* **2016**, *52*, 12430; b) M. E. Lee, S. M. Lee, J. Choi, D. Jang, S. Lee, H.-J. Jin, Y. S. Yun, *Small* **2020**, *16*, 2001053.

[14] a) Y. Zheng, Y. Wang, Y. Lu, Y.-S. Hu, J. Li, *Nano Energy* **2017**, *39*, 489; b) K. Gotoh, T. Yamakami, I. Nishimura, H. Kometani, H. Ando, K. Hashi, T. Shimizu, H. Ishida, *J. Mater. Chem. A* **2020**, *8*, 14472.

[15] D. A. Stevens, J. R. Dahn, *J. Electrochem. Soc.* **2000**, *147*, 1271.

[16] D. A. Stevens, J. R. Dahn, *J. Electrochem. Soc.* **2001**, *148*, A803.

[17] B. Zhang, C. M. Ghimbeu, C. Laberty, C. Vix-Guterl, J.-M. Tarascon, *Adv. Energy Mater.* **2016**, *6*, 1501588.

[18] Y. Cao, L. Xiao, M. L. Sushko, W. Wang, B. Schwenzer, J. Xiao, Z. Nie, L. V. Saraf, Z. Yang, J. Liu, *Nano Lett.* **2012**, *12*, 3783.

[19] a) Z. Li, C. Bommier, Z. S. Chong, Z. Jian, T. W. Surta, X. Wang, Z. Xing, J. C. Neuefeind, W. F. Stickle, M. Dolgos, P. A. Greaney, X. Ji, *Adv. Energy Mater.* **2017**, *7*, 1602894; b) S. Qiu, L. Xiao, M. L. Sushko, K. S. Han, Y. Shao, M. Yan, X. Liang, L. Mai, J. Feng, Y. Cao, X. Ai, H. Yang, J. Liu, *Adv. Energy Mater.* **2017**, *7*, 1700403.

[20] a) C. Bommier, T. W. Surta, M. Dolgos, X. Ji, *Nano Lett.* **2015**, *15*, 5888; b) Y. J. Jin, S. Sun, M. Ou, Y. Liu, C. Fan, X. Sun, J. Peng, Y. Li, Y. Qiu, P. Wei, Z. Deng, Y. Xu, J. Han, Y. Huang, *ACS Appl. Energy Mater.* **2018**, *1*, 2295; c) Z. V. Bobyleva, O. A. Drozhzhin, K. A. Dosaev, A. Kamiyama, S. V. Ryazantsev, S. Komaba, E. V. Antipov, *Electrochim. Acta* **2020**, *354*, 136647.

[21] G. Yang, X. Li, Z. Guan, Y. Tong, B. Xu, X. Wang, Z. Wang, L. Chen, *Nano Lett.* **2020**, *20*, 3836.
[22] Y. Liu, J. S. Xue, T. Zheng, J. R. Dahn, *Carbon* **1996**, *34*, 193.
[23] K. Gotoh, M. Maeda, A. Nagai, A. Goto, M. Tansho, K. Hashi, T. Shimizu, H. Ishida, *J. Power Sources* **2006**, *162*, 1322.
[24] E. M. Lotfabad, J. Ding, K. Cui, A. Kohandehghan, W. P. Kalisvaart, M. Hazelton, D. Mitlin, *ACS Nano* **2014**, *8*, 7115.
[25] K. Kubota, S. Shimadzu, N. Yabuuchi, S. Tominaka, S. Shiraishi, M. Abreu-Sepulveda, A. Manivannan, K. Gotoh, M. Fukunishi, M. Dahbi, S. Komaba, *Chem. Mater.* **2020**, *32*, 2961.
[26] a) M. Goktas, C. Bolli, E. J. Berg, P. Novák, K. Pollok, F. Langenhorst, M. V. Roeder, O. Lenchuk, D. Mollenhauer, P. Adelhelm, *Adv. Energy Mater.* **2018**, *8*, 1702724; b) P. K. Nayak, L. Yang, K. Pollok, F. Langenhorst, D. Aurbach, P. Adelhelm, *ChemElectroChem* **2019**, *6*, 2812; c) I. Escher, Y. Kravets, G. A. Ferrero, M. Goktas, P. Adelhelm, *Energy Technol.* **2021**, *9*, 2000880.
[27] Z. Li, Z. Jian, X. Wang, I. A. Rodriguez-Perez, C. Bommier, X. Ji, *Chem. Commun.* **2017**, *53*, 2610.
[28] H. Alptekin, H. Au, A. C. S. Jensen, E. Olsson, M. Goktas, T. F. Headen, P. Adelhelm, Q. Cai, A. J. Drew, M.-M. Titirici, *ACS Appl. Energy Mater.* **2020**, *3*, 9918.
[29] M. Dahbi, T. Nakano, N. Yabuuchi, T. Ishikawa, K. Kubota, M. Fukunishi, S. Shibahara, J.-Y. Son, Y.-T. Cui, H. Oji, S. Komaba, *Electrochem. Commun.* **2014**, *44*, 66.
[30] M. Goktas, C. Bolli, J. Buchheim, E. J. Berg, P. Novák, F. Bonilla, T. Rojo, S. Komaba, K. Kubota, P. Adelhelm, *ACS Appl. Mater. Interfaces* **2019**, *11*, 32844.
[31] N. Karimi, A. Varzi, S. Passerini, *Electrochim. Acta* **2019**, *304*, 474.
[32] a) A. Ponrouch, R. Dedryvere, D. Monti, A. E. Demet, J. M. A. Mba, L. Croguennec, C. Masquelier, P. Johansson, M. R. Palacin, *Energy Environ. Sci.* **2013**, *6*, 2361; b) A. Ponrouch, E. Marchante, M. Courty, J.-M. Tarascon, M. R. Palacin, *Energy Environ. Sci.* **2012**, *5*, 8572; c) S. Komaba, T. Ishikawa, N. Yabuuchi, W. Murata, A. Ito, Y. Ohsawa, *ACS Appl. Mater. Interfaces* **2011**, *3*, 4165.
[33] W. Zhang, M. Dahbi, S. Komaba, *Curr. Opin. Chem. Eng.* **2016**, *13*, 36.
[34] a) P. Bai, Y. He, P. Xiong, X. Zhao, K. Xu, Y. Xu, *Energy Storage Mater.* **2018**, *13*, 274; b) B. Xiao, F. A. Soto, M. Gu, K. S. Han, J. Song, H. Wang, M. H. Engelhard, V. Murugesan, K. T. Mueller, D. Reed, V. L. Sprenkle, P. B. Balbuena, X. Li, *Adv. Energy Mater.* **2018**, *8*, 1801441; c) J. Zhang, D.-W. Wang, W. Lv, S. Zhang, Q. Liang, D. Zheng, F. Kang, Q.-H. Yang, *Energy Environ. Sci.* **2017**, *10*, 370.
[35] P. Thomas, D. Billaud, *Electrochim. Acta* **2002**, *47*, 3303.
[36] F. A. Soto, P. Yan, M. H. Engelhard, A. Marzouk, C. Wang, G. Xu, Z. Chen, K. Amine, J. Liu, V. L. Sprenkle, *Adv. Mater.* **2017**, *29*, 1606860.
[37] R. D. Shannon, *Acta Crystallogr.* **1976**, *A32*, 751.
[38] T. Palaniselvam, B. Babu, H. Moon, I. Hasa, A. L. Santhosha, M. Goktas, Y.-N. Sun, L. Zhao, B.-H. Han, S. Passerini, A. Balducci, P. Adelhelm, *Batteries Supercaps* **2021**, *4*, 173.